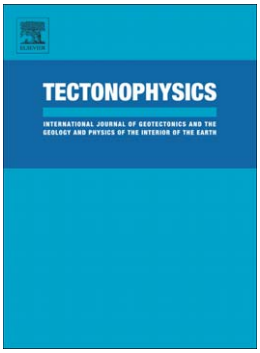

Subduction and volcanism in the Iberia-North Africa collision zone from tomographic images of the upper mantle

Antonio Villaseñor, Sébastien Chevrot, Mimoun Harnafi, Josep Gallart, Antonio Pazos, Inmaculada Serrano, Diego Córdoba, Javier A. Pulgar, Pedro Ibarra

PII: S0040-1951(15)00470-9
DOI: doi: 10.1016/j.tecto.2015.08.042
Reference: TECTO 126763

To appear in: *Tectonophysics*

Received date: 3 February 2015
Revised date: 24 July 2015
Accepted date: 25 August 2015

Please cite this article as: Villaseñor, Antonio, Chevrot, Sébastien, Harnafi, Mimoun, Gallart, Josep, Pazos, Antonio, Serrano, Inmaculada, Córdoba, Diego, Pulgar, Javier A., Ibarra, Pedro, Subduction and volcanism in the Iberia-North Africa collision zone from tomographic images of the upper mantle, *Tectonophysics* (2015), doi: 10.1016/j.tecto.2015.08.042

Subduction and volcanism in the Iberia-North Africa collision zone from tomographic images of the upper mantle

Antonio Villaseñor[1,*], Sébastien Chevrot[2], Mimoun Harnafi[3], Josep Gallart[1], Antonio Pazos[4], Inmaculada Serrano[5], Diego Córdoba[6], Javier A. Pulgar[7], Pedro Ibarra[8]

[1]Institute of Earth Sciences Jaume Almera, ICTJA-CSIC, 08028 Barcelona, Spain

[2]CNRS, Toulouse, France

[3]Institut Scientifique, Université Mohammed V Agdal, Rabat, Morocco

[4]Real Instituto y Observatorio de la Armada, San Fernando, Cádiz, España

[5]Instituto Andaluz de Geofísica, Universidad de Granada, España

[6]Universidad Complutense de Madrid, España

[7]Universidad de Oviedo, España

[8]IGME, Madrid, Spain

*email: antonio.villasenor@csic.es

Abstract

New tomographic images of the upper mantle beneath the westernmost Mediterranean suggest that the evolution of the region experienced two subduction-related episodes. First subduction of oceanic and/or extended continental lithosphere s, now located mainly beneath the Betics at depths greater than 400 km, took place on a NW-SE oriented subduction zone. This was followed by a slab-tear process that initiated in the east and propagated to the west, leading to westward slab rollback and possibly lower crustal delamination. The current position of the slab tear is located approximately at 4°W, and to the west of this location the subducted lithosphere is still attached to the surface along the Gibraltar arc. Our new P-wave velocity model is able to image the attached subducted lithosphere as a narrow high-velocity body extending to shallow depths, coinciding with the region of maximum curvature of the Gibraltar Arc, the occurrence of intermediate-depth earthquakes, and anomalously thick crust. This thick crust has a large influence in the measured teleseismic travel time residuals and therefore in the obtained P-wave tomographic model. We show that removing the effects of the thick crust significantly improves the shallow images of the slab and therefore the interpretations based on the seismic structure.

1. Introduction

The Gibraltar Arc, located in the western Mediterranean region, is the tightly curved western limit of the Alpine orogenic system (Figure 1). It is formed by the Betic chain in the southern Iberian Peninsula and the Rif mountains in northern Morocco. The arc, also referred to as the Betic-Rif system, encloses the Alboran Sea, a Neogene extensional basin.

The process or processes responsible for the formation and present-day structure of the Gibraltar Arc continue to be the subject of intense debate, with two major families of models being proposed: subduction-related processes (e.g. active subduction, slab rollback, slab tear, asymmetric delamination) and convective removal of the lithosphere (for a review of the different models see Platt et al., 2013 and references therein). A growing number of geophysical data collected in the last decade have improved our understanding of the region, predominantly favoring the slab rollback process, but still no single model has received a general consensus (see Gutscher et al., 2012; Platt et al., 2013 for recent reviews).

The Gibraltar Arc exhibits features that combined are characteristic (if not exclusive) of a subduction zone: deep seismicity, arc volcanism and an accretionary prism. Deep seismicity in the Betic-Rif is distributed in two zones: a slightly curved, N-S band of intermediate-depth events with foci between 70 and 120 km in the region of maximum curvature of the arc; and a tight cluster of deep-focus earthquakes beneath Granada with depths of about 625 km with two major events in 1954 (Mw 7.8, Chung and Kanamori, 1976) and 2010 (Mw 6.3, USGS). The intermediate-depth earthquakes dip very steeply to the center of the arc suggesting a small Wadati-Benioff zone. Their focal mechanisms are variable but indicate downdip tension (Ruiz-Constán et al., 2011). Volcanic rocks in the Alboran Basin are geochemically similar to volcanic rocks from active subduction zones (e.g. Izu–Bonin and Aeolian island arcs) and consist of low-K (tholeiitic) and medium- to high-K calc-alkaline series (Duggen et al., 2005). Finally, the Gulf of Cadiz, together with the western part of the external Rif and Betics have long been identified as an accretionary prism or wedge (e.g. Gutscher et al., 2009).

Another characteristic feature of most subduction zones is the existence of a positive P-wave velocity anomaly in the mantle that, in the case of the Alboran region,

extends continuously from shallow depths to the base of the transition zone (660 km seismic discontinuity). This feature has been identified by many authors (Blanco and Spakman, 1993; Calvert et al., 2000; Piromallo and Morelli, 2003; Spakman and Wortel, 2004) and has also been the subject of recent studies, some using a similar dataset to this one (Bezada et al., 2014; Bezada et al., 2013; Bonnin et al., 2014; Monna et al., 2013). Although most studies agree in the general shape of the anomaly, they differ in aspects that have important geodynamic implications. Is the high-velocity body attached to the surface and where? Do intermediate-depth earthquakes occur in regions of high or low P-wave velocity? Does the high velocity anomaly continue to the east along the coast of North Africa? Is the high velocity anomaly continuous or broken into different blocks?

In order to answer these questions, and to better understand the past and present-day evolution of the region, a number of projects have been carried out recently using different methodologies and approaches. As part of the TOPO-IBERIA project (2007-2013) the IberArray network, consisting of seismic, geodetic, and magnetotelluric instruments was deployed in Spain and Morocco (Díaz et al., 2009). In coordination with the seismic component of IberArray, which included approximately 200 sites equipped with broadband seismic instruments, other temporary broadband networks were deployed in Morocco, Spain, Portugal and France, filling coverage gaps in some regions and densifying others (Figure 1). Concurrently, permanent seismic monitoring networks in the western Mediterranean have increased the number of stations and upgraded their instrumentation to broadband, contributing to provide a very dense coverage of high-quality seismic stations.

The objective of this study is to make use of the waveform data from this large number of newly available broadband instruments to obtain improved images of the

mantle beneath the Gibraltar Arc and to address some of the unresolved geodynamical problems in the region.

2. Data

The data used in this study are *P*-wave arrival times of distant earthquakes recorded in broadband seismometers in the western Mediterranean region. In order to obtain very precise arrival times (both relative and absolute) we have first collected continuous waveform data for most of the permanent and temporary broadband stations operating in the Iberian Peninsula, Morocco and the Canary Islands from 2007 to 2012 both inclusive. We have then extracted from the continuous recordings time windows that include the theoretical first-arriving *P* wave, and used a phase picking method based on simulated annealing (Chevrot, 2002) that exploits the waveform similarity of distant events recorded on nearby stations.

2.1. Compilation of broadband seismograms

Permanent broadband networks in the region include both monitoring networks and research networks. Beginning in the 2000s most of the national monitoring networks in the region upgraded their instrumentation from short period to broadband, improved their real-time communications, and adopted GPS timing. These networks include those operated by the Instituto Geográfico Nacional (IGN, Spain, 55 broadband stations – all numbers are approximate and indicate the stations for which we have obtained waveform data), Instituto Português do Mar e da Atmosfera (IPMA, Portugal, 15 stations), Institut Cartogràfic i Geològic de Catalunya (ICGC, Catalonia, Spain, 17 stations), and Instituto Andaluz de Geofísica (IAG, Andalusia, Spain, 15 stations). Other relevant permanent research networks in the region are operated by the Spanish Royal Navy Observatory

(ROA) and the University of Lisbon. Finally individual stations from global and regional networks (GSN, GEOFON, MedNet) are also located in the study region (Figure 1).

While permanent networks in the region contribute a considerable number of stations (120 approximately), their distribution is not ideal for applying imaging methods based on teleseismic tomography. Stations are concentrated in the seismically active areas, resulting in a very heterogeneous coverage with large spatial variations in station density. The situation is worse in Morocco, where the coverage of permanent broadband stations is very sparse. To alleviate this problem the temporary network IberArray was designed to fill the gaps from permanent networks and provide an homogenous station spacing of 60 km in Spain. This was achieved in 3 consecutive deployments from south to north starting in 2007 and ending in 2013 that resulted in a total of 167 sites (Díaz et al., 2009; Figure 1). In addition 19 IberArray stations were installed in northern Morocco, and were later moved to the center and south, resulting in a total of 39 sites in Morocco.

Subsequently other temporary networks have been installed in Spain and Morocco both expanding and densifying the coverage of IberArray. The PASSCAL experiment PICASSO deployed 90 stations along a roughly north-south profile extending from the Iberian Massif and crossing the Strait of Gibraltar and the Atlas mountains (Figure 1). Additional stations deployed by the University of Münster, Germany (15) and Bristol, UK (6) have greatly improved the coverage in previously unsampled regions of the Atlas and Anti-Atlas mountains of southern Morocco (Figure 1).

Finally the Portuguese experiment WILAS and the French experiment PYROPE have extended the homogeneous coverage of IberArray into the western part of the Iberian Peninsula and southern and western France respectively. Data from these experiments have only recently become available and were not used in this study.

2.2 Data extraction and preparation

From this extensive dataset of more than 326 permanent and temporary broadband stations we have extracted *P* and *PKP* vertical component seismograms from teleseismic events with $M \geq 5.8$ recorded between 2008 and 2012. We apply to the selected seismograms a short period WWSSN filter (bandpass between 0.75 s and 1 s), and then we extract a time window starting 5 s before and ending 10 s after the theoretical arrival time of the first arrival (*P* or PKP_{df}), computed in the ak135 model (Kennett et al., 1995). A typical teleseismic event is recorded by approximately 250 stations.

2.3. Cluster analysis

Once the windows containing the *P* wave are extracted, a cluster analysis is performed, following the algorithm by Knuth (1968) which associates traces according to their degree of similarity, quantified with correlation coefficients. Since teleseismic *P* waves recorded by a regional array are expected to have similar waveforms, the main cluster contains all the traces for which we can reliably pick *P* wave onsets. This step is important, because it allows us to automatically reject poor data, simplifying the subsequent visual inspection of seismic traces.

2.2. Measurements of differential and absolute travel times

The waveform similarity of teleseismic *P* waves can also be exploited for accurately measuring relative arrival times by cross-correlation. The multichannel cross-correlation technique (MCCC) introduced by VanDecar and Crosson (1990) has been very popular to determine accurate relative arrival times of teleseismic waves recorded by regional arrays. However, this technique requires preliminary picks on each trace, that is both tedious and difficult to perform on noisy records. To keep the procedure automatic, we follow the approach introduced by Chevrot (2002) which consists in finding the

average waveform recorded by the array and the time delays at each station that minimize the misfit function:

$$E = \sum_{i=1}^{N} \sum_{j=1}^{M} \left| d_i(t_j) - s(t_j - \tau_i) \right|$$

where N is the number of seismograms, M is the number of samples, d_i is the observed record at station i, s is the average waveform, and τ_i its delay at station i. Note that we use a L_1 norm to reduce the effects of strong incoherent arrivals in the coda of the P wave. This minimization problem is solved by simulated annealing (Kirkpatrick et al., 1983). For more details on the algorithm we refer the reader to Chevrot (2002).

Once the minimum of the misfit function E has been found after a few thousands iterations all the records can be aligned with the average or reference waveform. We can then pick the absolute onset of the P wave on this reference waveform, which has larger signal-to-noise ratio than the individual recordings. Once we have obtained the absolute pick for the reference waveform, we can convert all the relative time delays τ_i to absolute, by simply adding them to the absolute pick. We thus measure both absolute and relative arrival times, with a precision comparable to measurements based on cross-correlations. However, by solving the global minimization problem E, we avoid getting trapped into secondary maxima of the correlation functions, as in the approach by VanDecar and Crosson (1990).

The results of this automatic processing are then visually inspected and outliers (e.g. stations with bad timing or wrong polarity) and noisy traces are eliminated. On average, it takes a couple of minutes to process an event recorded by about 250 stations. With this method it is possible to process efficiently large datasets to obtain clean and high quality travel time measurements. After analyzing the entire dataset, we kept 195

earthquakes from which a total of 13,366 *P* residuals and 482 PKP_{df} residuals were obtained.

2.3. Examples

In Figure 2 we show maps of the distribution of *P*-wave travel time residuals for two events occurring in different regions and therefore with different azimuths for the incoming *P* waves. The first event (Figure 2a) occurred in Svalbard and the azimuth is from the north. The distribution of the residuals is characterized by positive values (corresponding to late arrivals and therefore to seismic velocities slower than average) for most of the Betics and northern Rif. El Moudnib et al. (2015) show in their Figure 2b the distribution of residuals for a local earthquake in the region that is remarkably similar to the one observed in our Figure 2a, suggesting that these teleseismic late arrivals are most likely caused by crustal structure (i.e. sediments and thick crust). This strong signature of crustal structure in the distribution of residuals stresses the need for realistic crustal corrections, in order to correctly eliminate the influence of the crust and therefore obtain only the mantle structure.

A second event (Figure 2b) occurred in Afghanistan and with an azimuth from the east shows a pattern of the station residuals that is almost the opposite of the first event. The Betics and Rif are now characterized by negative residuals (corresponding to early arrivals and therefore to seismic velocities faster than average). This effect is most likely caused by the waves traveling through the high velocity anomaly located in the upper mantle beneath the Alboran region. This qualitative analysis of the travel time data emphasizes first the need for accurate crustal corrections, and second the existence of a significant signal from the upper mantle in the Alboran region.

3. Tomographic method

A detailed description of the methodology can be found in Chevrot et al. (2014). Here we describe only the most relevant aspects, and those that are specific of this study.

3.1. Crustal corrections

Teleseismic travel time residuals are affected by variations in crustal structure but their ability to resolve it are very limited. Therefore, the most common approach is to apply crustal corrections to the residuals to remove the effect of the crust and obtain a mantle-only model. This implies that crustal structure must be known independently (a priori).

The main issue with the computation of crustal corrections is the accuracy of the a priori crustal model. Global crustal models such as CRUST2.0 (Bassin et al., 2000) are not suitable to obtain accurate estimates of crustal effects on *P* residuals. An alternative is to consider more detailed regional crustal models. For the Iberian Peninsula, different crustal models are available in the literature. The model by Ziegler and Dèzes (2006) for western and central Europe has been constructed from a compilation of published regional Moho maps. The model by Gómez-Ortiz et al. (2011) has been derived from the map of gravity anomalies, whereas the model by Díaz and Gallart (2009) is based upon a compilation of deep seismic sounding studies in the Iberian Peninsula. While this last source of information is probably the most reliable, their final crustal model appears to be distorted in poorly sampled regions by the interpolation method used. A simple comparison of these models reveals that they give very different pictures of the crustal roots beneath the Betics, with highly variable amounts of crustal thickening.

Because of this large variability in published crustal models we have thus decided to construct a new crustal model from the compilation of the raw estimates coming from seismic profiles made by Díaz and Gallart (2009) and from crustal thicknesses estimated

using receiver functions (e.g. Mancilla et al., 2013; Mancilla et al., 2012). To fill the gaps, we have computed receiver functions at other stations with available waveform data for which we determined the Moho depth. Figure 3 shows the map of apparent crustal thickness obtained by interpolating the complete dataset over a regular 0.05° grid. The main feature in the crustal map is the existence of thick crust beneath the Betic-Rif system, particularly in the most curved part of the Gibraltar arc. Crustal thickness there can reach more than 45 km, while the average crustal thickness in the stable part of Iberia is approximately 31 km, close to the standard 35 km crustal thickness in the ak135 reference Earth model (Kennett et al., 1995).

3.2. Model parameterization and inversion

The tomographic model is parameterized in a spherical grid with homogeneous blocks of dimension of 0.25° in latitude and longitude, and 25 km in depth, down to 900 km depth. Rays are traced in the ak135 reference Earth model (Kennett et al., 1995). Following an algorithm similar to Spakman and Bijwaard (2001), we construct an irregular block model which agglomerates the small blocks of the initial regular grid in the poorly sampled parts of the model. This construction reduces the size of the inverse problem and improves its conditioning. To regularize the inversion, we add penalty conditions on the L_2 norm and on the Laplacian of the tomographic model. The variance reduction obtained after 500 iterations of the LSQR algorithm (Paige and Saunders, 1982) is around 70%. This rather large reduction of travel time residuals is a strong indication of the quality of our data set and of the low level of noise in the travel time measurements.

4. Results

4.1. Effects of crustal corrections

Including crustal corrections in addition to ellipticity and station elevation corrections improves the variance reduction by about 4%,which is quite significant. Figure 4 shows the comparison of the model results obtained with and without crustal corrections for two selected depth layers of the model (75-100 km and 125-150 km). The differences are more significant for the shallowest layers of the model, but the effect of not taking into account crustal structure can extend to greater depths.

4.2. Resolution

We have evaluated the resolving power of our dataset using checkerboard reconstruction tests. In Figure 5 we show the results of these tests, for anomalies with sizes of 1°. As it can be observed in those figures, reconstruction of the checkerboard pattern is very good in the uppermost mantle for the southern Iberian Peninsula and northern Morocco, including the Alboran region. The region with good reconstruction of the synthetic anomalies becomes larger for deeper layers, which is consistent with the increase in the area with crossing rays.

4.3. Model description

In Figure 6 we show several horizontal slices of the final model from the uppermost mantle to the bottom of the transition zone. At all depths, the most conspicuous feature is the high velocity body located beneath the Alboran basin and the Betic cordillera. Down to 200 km this high velocity body has an arcuate shape, coinciding with the most curved segment of the Betic-Rif chain, but shifted to the east. With depth, the anomaly tends to move towards the east, giving the appearance of an east-dipping slab (upper 300 km in Figure 7a). However, with increasing depth, the anomaly starts to lose

the arcuate shape and even seems to break into blobs (see for examples Figures 6c and 6d). Below 400 km the anomaly seems to be continuous again and, instead of curved, exhibits a linear character with a NE-SW orientation coincident with the orientation of the Betic cordillera. Other high velocity anomalies but with smaller amplitudes are observed beneath the Iberian Massif and Moroccan Meseta.

In addition to the high velocity anomalies, multiple, smaller low velocity anomalies occur throughout the region. Most of these anomalies correspond to regions with Neogene volcanism (e.g. Figure 6a). Although there is a general good correspondence, some volcanic areas (Calatrava, Cabo de Gata) are located in the edges of the low velocity anomalies, not in the center. Similarly a small but prominent low velocity anomaly beneath the Strait of Gibraltar is not associated with surface volcanism.

5. Discussion

Here we will describe the robust, most prominent features of the *P*-wave velocity model and discuss their geodynamic implications. We will also compare our model with previous studies not only to identify the common characteristics, but also to emphasize the new features found. A particularly useful comparison will be with the model of (Villaseñor et al., 2003), hereafter referred to as VSE03, because of its complementary characteristics to the one presented here. Both models are based on *P*-wave arrival times but the dataset and methodology used are independent. VSE03 uses the same methodology of Bijwaard et al. (1998) with a greatly increased regional and teleseismic dataset of arrival times from earthquakes occurred between 1964-2002 reported by the ISC and relocated with the EHB method (Engdahl et al., 1998). For comparison, the model presented here uses teleseismic arrival times from earthquakes that occurred between 2008-2012 and measured by us, mostly in temporary broadband stations. Both

tomographic methods use ray theory but while in this study we invert relative *P* and PKP_{df} arrival times in a regional model, in VSE03 absolute arrival times of *P*, *PKP*, and depth phases (*pP*, *pwP*) were inverted in a global model (a detailed comparison of both models is shown in the Supplementary Material). Other relevant models for comparison are those of Bezada et al. (2014); Bezada et al. (2013) and Bonnin et al. (2014) that were obtained using a similar dataset but with a finite frequency approach instead of ray theory. Monna et al. (2013) provide another recent teleseismic *P*-wave model that incorporates a new dataset from a temporary OBS deployment in the Gulf of Cadiz and has therefore improved resolution in that region.

As has been seen in previous studies, the most conspicuous feature in the region is a high-velocity anomaly located mainly beneath the Alboran Sea and Betics that extends from the top of the mantle down to the bottom of the transition zone (i.e. the 660 km discontinuity) and is interpreted here as a subducted slab or slabs.

In its shallow part this anomaly has an arcuate shape, mimicking the curvature of the Gibraltar arc. Although teleseismic models such as this one are not very reliable for imaging the most shallow layers, there seems to be a clear boundary at approximately 4°W that separates high velocities beneath the western Betics from low velocities to the east. At approximately this location a number of recent studies based on different kinds of geophysical data propose the existence of a tear in the slab: Rosell et al. (2011) using magnetotelluric data; Ruiz-Constán et al. (2011) using focal mechanisms of intermediate-depth earthquakes; Mancilla et al. (2013) using receiver functions and GPS. With increasing depth we observe that the eastern limit of the high velocity anomaly (Alboran slab) beneath Spain moves progressively towards the east (Figures 6 and 8). This geometry is also seen in VSE03 as shown in Garcia-Castellanos and Villaseñor (2011) and the Supplementary Material, and in Bezada et al. (2013) and Monna et al. (2013). This is

consistent with a west-propagating slab tear, with its current location at approximately 4°W beneath the western Betics. Slab contours shown in Figure 8 also seem to suggest another tear in the southern side of the slab, along the Moroccan coast, although much shorter in length. The existence of a northern and southern tear would provide an explanation for the change in magma chemistry along the margins of the Alboran Sea (Duggen et al., 2003), for the long duration of the shallow connection between the Mediterranean and the Atlantic needed to explain the large amount of salt precipitated during the Messinian Salinity crisis, and for the later closure of those connections and subsequent desiccation of the Mediterranean (Garcia-Castellanos and Villaseñor, 2011).

Between 75 and 175 km depth (Figures 6a and 6b) the high velocity anomaly defines a continuous and narrow slab (less than 100 km thick on a horizontal cross section) with an asymmetric crescent shape (the northern or Betic branch extending more to the east than the southern or Rif branch). In this depth range, earthquake hypocenters are clearly located within the high-velocity anomaly (Figure 7). Although this is the most frequent observation in subducting slabs elsewhere, previous studies in this region (including VSE03) have found the intermediate-depth seismicity associated with low velocities, leading to interpretation as subducted or delaminated continental crust (e.g. Morales et al., 1999; Valera et al., 2008). The probable reason for obtaining low velocities in the vicinity of the Alboran intermediate-depth earthquakes (at least in the case of VSE03) is not taking into account crustal corrections, which are particularly important in that region, where an unusually thick crust has been found (Figure 3). The result obtained here that intermediate-depth earthquakes occur inside the high velocity anomaly, and therefore inside the slab, does not rule out the existence of continental subduction and/or delamination. In fact these two processes are a plausible explanation for the observation of

an anomalously thick crust (> 50 km) in the westernmost Gibraltar arc (Mancilla et al., 2013), where topography is relatively low.

In Figure 8 we have drawn contours of the top of the slab from 100 to 400 km depth (defined here when the high velocity anomaly reaches a value of +1%). These contours show an east-dipping, 200 km wide slab. The curvature of the slab decreases to the east, while its steepness increases in that direction. This geometry is consistent with a process of rollback of a narrow slab towards the west. This rollback process is still currently active, as evidenced by GPS and focal mechanisms of local earthquakes in the western Rif and Betics (Fadil et al., 2006; Koulali et al., 2011; Mancilla et al., 2013; Palano et al., 2013; Perouse et al., 2010).

Below 400 km there is a change in the shape of the high velocity anomaly. The predominant shift of the high velocity anomaly to the east with increasing depth is replaced by a near-vertical SW-NE trending anomaly located beneath the Alboran Sea and most of the Betic range (Figures 6, 8). The western limit of the anomaly from 400 to 660 km is approximately constant at 5.5°W, while it widens and extends toward the east with increasing depth. This change in slab geometry below 400 km depth suggests the existence of at least two subduction stages: first the subduction of Ligurian-Thetis lithosphere in a NW-dipping (e.g. Faccenna et al., 2004) or a SE-dipping direction (Vergés and Fernandez, 2012), followed by east-dipping subduction and westward slab rollback. This change in subduction is also in agreement with the observed ages and directions of extension in the Alboran region. The most recent (from ~27 to 9 Ma) and faster extension episode in the Alboran basin has an E-W direction, consistent with backarc extension caused by westward slab rollback. This was preceded by a less pronounced NNW-SSE extensional episode (Martínez-Martínez and Azañón, 2002), in a direction perpendicular to the deep high velocity anomaly. In both cases the extension

directions are orthogonal to the strike of the subduction, consistent with a mechanism of backarc extension.

The geometry of the slab below 400 km has also an important implication for the validation of proposed evolution models for the westernmost Mediterranean. Models that propose exclusively westward slab rollback to explain the current configuration of the Alboran region (e.g. Faccenna et al., 2004; Rosenbaum et al., 2002) are compatible with the seismic structure observed down to 400 km. However, westward slab rollback alone cannot explain the presence of high velocity material in the transition zone beneath the western Alboran sea, right below the position where the slab is currently attached to the surface (e.g. El Moudnib et al., 2015; Mancilla et al., 2013). The position of the deep high velocity anomaly beneath the Alboran basin and the Betics (Figure 8) and the absence of high velocity anomalies beneath northern Africa east of 2°W at any depth, suggests that this slab was attached to the Iberian lithosphere and subducted in SSE direction beneath Africa. However from the evidence presented here we cannot rule out the opposite scenario (e.g. Faccenna et al., 2004; Rosenbaum et al., 2002). In fact the N-S cross section of our model shown in Figure 7b illustrates a near vertical slab below 300 km depth, but with a small northward dip, compatible with northward subduction of Africa beneath Iberia.

In addition to the high velocity anomalies associated with the Alboran slab, our model also exhibits regions of significant low velocity anomalies (less than 1%). Since the anomalies in our model are referred to the layer average, these may not be actual low velocities with respect to global averages such as PREM or ak135. However, comparison of the low velocities of our model with those in VSE03 (which are referred to ak135) show that they coincide well in location and amplitude indicating that they are actual relative low velocities with respect to the global average (see Supplementary Material).

This confirms that there is very little deviation of the average velocity in our regional model from the global average, as expected from the large extent of the region covered in our study. Amplitudes of low velocity anomalies in ray-based travel time models are known to be underestimated (e.g. due to wavefront healing), therefore the values presented here are lower bounds of the absolute value of the anomalies. This has to be taken into account when using seismic velocity anomalies obtained with this methodology to infer thermal and compositional variations.

Since a likely origin of low velocities in the mantle is higher temperatures with respect to the surrounding mantle, we compare the location of the most significant low velocity anomalies with areas of recent volcanism and proposed thin lithosphere.

In the uppermost mantle (i.e. above 250 km) there are four well defined regions of relative low velocities that surround the Alboran Sea high velocity anomaly (Figure 6a,b). Three of them coincide remarkably well with areas of Neogene volcanism: Levante-Valencia Trough, eastern Rif, and Middle Atlas. A fourth anomaly, possibly connected to the Middle Atlas anomaly, extends beneath the Gibraltar Strait and eastern Gulf of Cadiz, but does not exhibit any surface expression of recent volcanism. These features have already been described in previous tomographic studies based on travel times (Bezada et al., 2014; Bezada et al., 2013; Bonnin et al., 2014) and surface wave dispersion (Palomeras et al., 2014).

The first and largest of these anomalies, the Levante-Valencia Trough, is centered approximately on the northeastern end of the Betic range. This low velocity region probably extends eastwards beneath the Valencia Trough (as observed in VSE03) but our dataset does not have sufficient sampling in that region. From west to east and following an ENE trend, the Campo de Calatrava, Cofrentes-Picasent, and Valencia Trough volcanic fields are associated with this anomaly. The Campo de Calatrava volcanic province is

located in the western edge of the anomaly near the southeastern limit of the Iberian Massif, while the much smaller Cofrentes-Picasent volcanics coincide with the center of the anomaly. Although here the absolute values of the anomaly are the largest, the volume of erupted material is small, and the heat flow values in the area and other geothermal indicators are not significantly large (e.g. Fernandez et al., 1998). The low velocity anomaly extends eastward into the Valencia Trough, where numerous submarine volcanic outcrops exist, emerging in the Columbretes Islands (e.g. Martí et al., 1992). This low velocity anomaly extends down to approximately 300 km depth, both in our model and in VSE03. At greater depths, low velocities decrease in magnitude and move to the central Iberian Peninsula.

The second largest low velocity anomaly in size is located beneath the Middle Atlas (see also Bezada et al., 2014; Palomeras et al., 2014). In this case the location of the maximum absolute value of the anomaly coincides with the location of the Middle Atlas basaltic province, which is the area of largest and youngest volcanism in Morocco, covering a surface of ca. 960 km^2 (El Azzouzi et al., 2010). The volcanism in this region has been proposed as the result of a thin lithosphere (less than 90 km) leading to an asthenospheric uprising (El Azzouzi et al., 2010; Fullea et al., 2010). This coincides well with our model and other recent ones (Bezada et al., 2014; Palomeras et al., 2014), that shows here well defined low velocities from 70 to 200 km depth. Below that depth, low velocities fade out and are replaced by a small-amplitude high-velocity zone down to the top of the transition zone.

Three other anomalies branch out from the Middle Atlas low velocity anomaly: to the NNW (Strait of Gibraltar - Gulf of Cadiz), NE (eastern Rif) and SW (High Atlas - Anti-Atlas). The NNW anomaly, in spite of large absolute values in the top 200 km, has no associated surface volcanism. The NE anomaly coincides with the eastern Rif volcanic

fields of Guelliz, Gourougou and Oujda. The easternmost Oujda field is in the center of the anomaly, while Guelliz and Gourougou, located more to the west, border with the Alboran Sea high velocity anomaly. Finally, the SW anomaly follows the trend of the central and western High Atlas and northern Anti-Atlas. This is in good agreement with lithospheric modeling results (e.g. Fullea et al., 2010; Teixell et al., 2005) that indicate the presence of thin lithosphere (< 100 km) beneath these regions. This would explain not only the observed low velocity anomalies, but other features such as high topography with modest tectonic shortening, the absence of large crustal roots to support elevation, and the occurrence of alkaline magmatism contemporaneous to compression in the volcanic provinces of the Middle Atlas and Anti-Atlas (Siroua,11-2 Ma; Saghro, 9.6-2.9 Ma).

At depths greater than 300 km the correlation between low velocity anomalies and Cenozoic volcanism begins to disappear. The only exception occurs beneath the Anti-Atlas, where the absolute value of the anomaly even intensifies with depth. Since this area is on the edge of our model, this anomaly could be the result of smearing in the vertical direction because of the lack of crossing rays. For the same reason we cannot confirm the continuation of this low velocity anomaly to the west into the Canary Islands, as the model below 300 km seems to indicate. Some authors have proposed the existence of a corridor in the sublithospheric mantle extending from the Canary Islands to the Alboran sea that would be responsible for the observed Cenozoic volcanism in Morocco (Duggen et al., 2009). Oyarzun et al. (1997) propose that volcanism in western North Africa and in the European Cenozoic rift systems (Goes et al., 1999; Ziegler, 1992) might be caused by a single, long-lived mantle upwelling. Our results support a single low velocity anomaly extending from at least the westernmost Atlas (and possibly from the Canary Islands) to the Alboran Sea. This anomaly, however seems to be disconnected from the Levante-Valencia Trough anomaly by the high velocities of the Alboran slab and the Iberian

Massif. The resulting structure would be of two independent, roughly SW-NE trending low velocity anomalies. This geometry is also observed in VSE03, where the Levante-Valencia Trough anomaly continues north into the Central European volcanic province.

6. Conclusions

We have obtained new images of the upper mantle beneath the westernmost Mediterranean region using teleseismic travel time tomography. We have used a new dataset of high-quality P-wave arrival times recorded on permanent and temporary broadband instruments in the region. Due to the higher quality and coverage of the new dataset, we are able to define with more detail features that were observed in previous models based on ISC arrival times. The dominant feature of the model is a high velocity anomaly that extends from the base of the crust down to the 660 km discontinuity. We interpret this anomaly as subudcted lithospheric slab or slabs. The deepest part of the anomaly (below 400 km depth) would correspond to a SW-NE oriented subduction zone (dipping either to the NW or the SE) that would have consumed all the available oceanic lithosphere of the Ligurian Tethys between Iberia and Africa. A second episode of westward slab rollback would be responsible for the formation of the Alboran basin and the velocity anomaly observed above 400 km depth. Currently this anomaly is attached to the Iberian plate, but only in the westernmost part of the Gibraltar arc.

Teleseismic tomography using ray theory cannot recover accurately the magnitude of the velocity anomalies (particularly low velocities). However, with the ray coverage of our dataset, the parameterization, smoothing, and crustal corrections used, we are able to resolve small scale features, such as an arcuate, concave to the east, high velocity slab-like anomaly that exactly coincides with the geometry of the intermediate depth seismicity (Figure 6a).

We also find a clear relationship between shallow low velocity regions and volcanism. All significant low velocity anomalies (with the exception of the Strait of Gibraltar-Gulf of Cadiz anomaly) contain recent volcanic fields and, conversely, no recent volcanic field occur in regions of shallow high velocity anomalies. However, in some cases volcanic fields are located in the edges of the anomalies, while in others in the region of maximum absolute value of the anomaly. This indicates that temperature alone is not the only controlling factor of surface volcanism, or that not all low velocity anomalies are caused by thermal anomalies, and differences in composition might play a role.

Acknowledgements

We thank the operators of the permanent networks in the region for providing part of the waveform data used in this study: Instituto Geográfico Nacional (IGN, Spain), Instituto Andaluz de Geofísica (IAG, Spain), Real Instituto y Observatorio de la Armada (ROA, Spain), Institut Cartogràfic i Geològic de Catalunya (ICGC), and Instituto Português do Mar e da Atmosfera (IPMA, Portugal). Data from other individual stations have been obtained from the ORFEUS (The Netherlands), GEOFON (Germany) and IRIS (USA) data centers. We also thank Arie van den Berg and Jeannot Trampert from Utrecht University for contributing to the IberArray deployment with the NARS stations, and Tine Thomas (Münster University, Germany) and James Wookey (University of Bristol, UK) for contributing the data from their temporary network in Morocco. This is a contribution of the Team Consolider- Ingenio 2010 TOPO-IBERIA (CSD2006-00041). Additional funding was provided by the SIBERIA (CGL2006-01171), RIFSIS (CGL2009-09727) and ALERTES-RIM (CGL2013-45724-C3-3-R) projects.

References

Bassin, C., Laske, G., Masters, G., 2000, The current limits of resolution for surface wave tomography in North America, Eos Trans. AGU, Vol. 81, F897, AGU Fall Meeting,

Bezada, M.J., Humphreys, E.D., Davila, J.M., Carbonell, R., Harnafi, M., Palomeras, I., Levander, A., 2014. Piecewise delamination of Moroccan lithosphere from beneath the Atlas Mountains. Geochemistry Geophysics Geosystems 15, 975-985.

Bezada, M.J., Humphreys, E.D., Toomey, D.R., Harnafi, M., Davila, J.M., Gallart, J., 2013. Evidence for slab rollback in westernmost Mediterranean from improved upper mantle imaging. Earth and Planetary Science Letters 368, 51-60.

Bijwaard, H., Spakman, W., Engdahl, E.R., 1998. Closing the gap between regional and global travel time tomography. Journal of Geophysical Research 103, 30055-30078.

Blanco, M.J., Spakman, W., 1993. The P-wave velocity structure of the mantle below the Iberian Peninsula: evidence for subducted lithosphere below southern Spain. Tectonophysics 221, 13-34.

Bonnin, M., Nolet, G., Villaseñor, A., Gallart, J., Thomas, C., 2014. Multiple-frequency tomography of the upper mantle beneath the African/Iberian collision zone. Geophysical Journal International 198, 1458-1473.

Calvert, A., Sandvol, E., Seber, D., Barazangi, M., Roecker, S., Mourabit, T., Vidal, F., Alguacil, G., Jabour, N., 2000. Geodynamic evolution of the lithosphere and upper mantle beneath the Alboran region of the western Mediterranean: Constraints from travel time tomography. Journal of Geophysical Research 105, 10871-10898.

Chevrot, S., 2002. Optimal measurement of relative and absolute delay times by simulated annealing. Geophysical Journal International 151, 164-171.

Chevrot, S., Villaseñor, A., Sylvander, M., Benahmed, S., Beucler, E., Cougoulat, G., Delmas, P., de Saint Blanquat, M., Díaz, J., Gallart, J., Grimaud, F., Lagabrielle, Y., Manatschal, G., Mocquet, A., Pauchet, H., Paul, A., Pequegnat, C., Quillard, O., Roussel, S., Ruiz, M., Wolyniec, D., 2014. High-resolution imaging of the Pyrenees and Massif Central from the data of the PYROPE and IBERARRAY portable array deployments. Journal of Geophysical Research: Solid Earth 119, 6399-6420.

Chung, W.Y., Kanamori, H., 1976. Source process and tectonic implications of the Spanish deep-focus earthquake of March 29, 1954. Physics of the Earth and Planetary Interiors 13, 85-96.

Díaz, J., Gallart, J., 2009. Crustal structure beneath the Iberian Peninsula and surrounding waters: A new compilation of deep seismic sounding results. Phys. Earth Planet. Inter. 173, 181-190.

Díaz, J., Villaseñor, A., Gallart, J., Morales, J., Pazos, A., Córdoba, D., Pulgar, J.A., García-Lobón, J.L., Harnafi, M., Group, T.-I.S.W., 2009. The IBERARRAY broadband seismic network: a new tool to investigate the deep structure beneath Iberia. Orfeus Newsl. 8, 1-6.

Duggen, S., Hoernle, K., Hauff, F., Klugel, A., Bouabdellah, M., Thirlwall, M., 2009. Flow of Canary mantle plume material through a subcontinental lithospheric corridor beneath Africa to the Mediterranean. Geology 37, 283-286.

Duggen, S., Hoernle, K., van den Bogaard, P., Garbe-Schönberg, D., 2005. Post-Collisional Transition from Subduction- to Intraplate-type Magmatism in the Westernmost Mediterranean: Evidence for Continental-Edge Delamination of Subcontinental Lithosphere. Journal of Petrology 46, 1155-1201.

Duggen, S., Hoernle, K., van den Bogaard, P., Rüpke, L.H., Phipps Morgan, J., 2003. Deep roots of the Messinian salinity crisis. Nature 422, 602-606.

El Azzouzi, M., Maury, R.C., Bellon, H., Youbi, N., Cotten, J., Kharbouch, F., 2010. Petrology and K-Ar chronology of the Neogene-Quaternary Middle Atlas basaltic province, Morocco. Bulletin de la Société Géologique de France 181, 243-257.

El Moudnib, L., Villaseñor, A., Harnafi, M., Gallart, J., Pazos, A., Serrano, I., Córdoba, D., Pulgar, J.A., Ibarra, P., Himmi, M.M., Chourak, M., 2015. Crustal structure of the Betic–Rif system, western Mediterranean, from local earthquake tomography. Tectonophysics 643, 94-105.

Engdahl, E.R., van der Hilst, R.D., Buland, R.P., 1998. Global teleseismic earthquake relocation with improved travel times and procedures for depth determination. Bulletin of the Seismological Society of America 88, 722-743.

Faccenna, C., Piromallo, C., Crespo-Blanc, A., Jolivet, L., Rosseti, F., 2004. Lateral slab deformation and the origin of the western Mediterranean arcs. Tectonics 23, TC1012.

Fadil, A., Vernant, P., McClusky, S., Reilinger, R., Gomez, F., Ben Sari, D., Mourabit, T., Feigl, K.L., Barazangi, M., 2006. Active tectonics of the western Mediterranean: Geodetic evidence for rollback of a delaminated subcontinental lithospheric slab beneath the Rif Mountains, Morocco. Geology 34, 529.

Fernandez, M., Marzán, I., Correia, A., Ramalho, E., 1998. Heat flow, heat production, and lithospheric thermal regime in the Iberian Peninsula. Tectonophysics 291, 29-53.

Fullea, J., Fernandez, M., Afonso, J.C., Vergés, J., Zeyen, H., 2010. The structure and evolution of the lithosphere–asthenosphere boundary beneath the Atlantic–Mediterranean Transition Region. Lithos 120, 74-95.

Garcia-Castellanos, D., Villaseñor, A., 2011. Messinian salinity crisis regulated by competing tectonics and erosion at the Gibraltar arc. Nature 480, 359-363.

Goes, S., Spakman, W., Bijwaard, H., 1999. A lower mantle source for central European volcanism. Science 286, 1928-1931.

Gómez-Ortiz, D., Agarwal, B.N.P., Tejero, R., Ruiz, J., 2011. Crustal structure from gravity signatures in the Iberian Peninsula. Geol. Soc. Am. Bull. 123, 1247-1257.

Gutscher, M.-A., Dominguez, S., Westbrook, G.K., Leroy, P., 2009. Deep structure, recent deformation and analog modeling of the Gulf of Cadiz accretionary wedge: Implications for the 1755 Lisbon earthquake. Tectonophysics 475, 85-97.

Gutscher, M.A., Dominguez, S., Westbrook, G.K., Le Roy, P., Rosas, F., Duarte, J.C., Terrinha, P., Miranda, J.M., Graindorge, D., Gailler, A., Sallares, V., Bartolome, R., 2012. The Gibraltar subduction: A decade of new geophysical data. Tectonophysics 574-575, 72-91.

Kennett, B.L.N., Engdahl, E.R., Buland, R., 1995. Constraints on seismic velocities in the Earth from traveltimes. Geophys. J. Int. 122, 108-124.

Kirkpatrick, S., Gelatt, C.D., Vecchi, M.P., 1983. Optimization by simulated annealing. Science 220, 671-680.

Knuth, D.E., 1968. The Art of Computer Programming. Addison-Wesley, Reading, Mass.

Koulali, A., Ouazar, D., Tahayt, A., King, R.W., Vernant, P., Reilinger, R.E., Mcclusky, S., Mourabit, T., Martín Dávila, J., Amraoui, N., 2011. New GPS constraints on active deformation along the Africa–Iberia plate boundary. Earth Planet. Sci. Lett. 308, 211-217.

Mancilla, F., Stich, D., Berrocoso, M., Martin, R., Morales, J., Fernández-Ros, A., Paez, R., Pérez-Peña, A., 2013. Delamination in the Betic Range: Deep structure, seismicity, and GPS motion. Geology 41, 307-310.

Mancilla, F.d.L., Stich, D., Morales, J., Julià, J., Díaz, J., Pazos, A., Córdoba, D., Pulgar, J.A., Ibarra, P., Harnafi, M., Gonzalez-Lodeiro, F., 2012. Crustal thickness variations in northern Morocco. J. Geophys. Res. 117, B02312.

Martí, J., Mitjavila, J., Roca, E., Aparicio, A., 1992. Cenozoic magmatism of the Valencia trough (western Mediterranean): relationship between structural evolution and volcanism. Tectonophysics 203, 145-165.

Martínez-Martínez, J.M., Azañón, J.M., 2002. Orthogonal extension in the hinterland of the Gibraltar Arc (Beltics, SE Spain). Journal of the Virtual Explorer 8, 1-20.

Monna, S., Cimini, G.B., Montuori, C., Matias, L., Geissler, W.H., Favali, P., 2013. New insights from seismic tomography on the complex geodynamic evolution of two adjacent domains: Gulf of Cadiz and Alboran Sea. Journal of Geophysical Research: Solid Earth 118, 1587-1601.

Morales, J., Serrano, I., Jabaloy, A., Galindo-Zaldívar, J., Zhao, D., Torcal, F., Vidal, F., González-Lodeiro, F., 1999. Active continental subduction beneath the Betic Cordillera and the Alborán Sea. Geology 27, 735-738.

Oyarzun, R., Doblas, M., López-Ruiz, J., Cebriá, J.M., 1997. Opening of the central Atlantic and asymmetric mantle upwelling phenomena: Implications for long-lived magmatism in western North Africa and Europe. Geology 25, 727-730.

Paige, C.C., Saunders, M.A., 1982. LSQR: An algorithm for sparse linear equations and sparse least squares. ACM Trans. Math. Software 8, 43-71.

Palano, M., González, P.J., Fernández, J., 2013. Strain and stress fields along the Gibraltar Orogenic Arc: Constraints on active geodynamics. Gondwana Research 23, 1071-1088.

Palomeras, I., Thurner, S., Levander, A., Liu, K., Villaseñor, A., Carbonell, R., Harnafi, M., 2014. Finite-frequency Rayleigh wave tomography of the western Mediterranean: Mapping its lithospheric structure. Geochemistry Geophysics Geosystems 15, 140-160.

Perouse, E., Vernant, P., Chery, J., Reilinger, R., Mcclusky, S., 2010. Active surface deformation and sub-lithospheric processes in the western Mediterranean constrained by numerical models. Geology 38, 823-826.

Piromallo, C., Morelli, A., 2003. P wave tomography of the mantle under the Alpine-Mediterranean area. Journal of Geophysical Research 108, 2065.

Platt, J.P., Behr, W.M., Johanesen, K., Williams, J.R., 2013. The Betic-Rif Arc and Its Orogenic Hinterland: A Review. Annual Reviews in Earth and Planetary Sciences 41, 313-357.

Rosell, O., Martí, A., Marcuello, À., Ledo, J., Queralt, P., Roca, E., Campanyà, J., 2011. Deep electrical resistivity structure of the northern Gibraltar Arc (western Mediterranean): evidence of lithospheric slab break-off. Terra Nova 23, 179-186.

Rosenbaum, G., Lister, G.S., Duboz, C., 2002. Reconstruction of the tectonic evolution of the western Mediterranean since the Oligocene. Journal of the Virtual Explorer 8, 107-130.

Ruiz-Constán, A., Galindo-Zaldívar, J., Pedrera, A., Célérier, B., Marín-Lechado, C., 2011. Stress distribution at the transition from subduction to continental collision (northwestern and central Betic Cordillera). Geochem. Geophys. Geosyst. 12, Q12002.

Spakman, W., Bijwaard, H., 2001. Optimization of cell parameterizations for tomographic inverse problems. Pure and Applied Geophysics 158, 1401-1423.

Spakman, W., Wortel, M.J.R., 2004. A tomographic view on Western Mediterranean Geodynamics, in: Cavazza, W., Roure, F., Spakman, W., Stampfli, G.M., Ziegler,

P.A. (Eds.), The TRANSMED Atlas, The Mediterranean Region from Crust to Mantle, pp. 31-52.

Teixell, A., Ayarza, P., Zeyen, H., Fernandez, M., Arboleya, M.-L., 2005. Effects of mantle upwelling in a compressional setting: the Atlas Mountains of Morocco. Terra Nova 17, 456-461.

Valera, J.L., Negredo, A.M., Villaseñor, A., 2008. Asymmetric delamination and convective removal numerical modeling: comparison with evolutionary models for the Alboran Sea region. Pure and Applied Geophysics 165, 1683-1706.

VanDecar, J.C., Crosson, R.S., 1990. Determination of teleseismic relative phase arrival times using multi-channel cross-correlation and least squares. Bulletin of the Seismological Society of America 80, 150-169.

Vergés, J., Fernandez, M., 2012. Tethys–Atlantic interaction along the Iberia–Africa plate boundary: The Betic–Rif orogenic system. Tectonophysics 579, 144-172.

Villaseñor, A., Spakman, W., Engdahl, E.R., 2003, Influence of regional travel times in global tomographic models, Geophysical Research Abstracts, Vol. 5, EAE03-A-08614, EGS-AGU-EUG Joint Assembly, Nice, France.

Ziegler, P.A., 1992. European Cenozoic rift system. Tectonophysics 208, 91-111.

Ziegler, P.A., Dèzes, P., 2006. Crustal Evolution of Western and Central Europe. Geol. Soc. London Mem. 32, 43-56.

Figure captions

Figure 1. Location map of the study region showing the different structural units. The broad-band stations used are shown as triangles and color coded according to the network. CC: Campo de Calatrava volcanics, Cf: Cofrentes, CG: Cabo de Gata volcanics, Col: Columbretes Islands, GGO: Guelliz, Gourougou and Oujda volcanics, MA: Middle Atlas, Pc: Picassent.

Figure 2. Examples of distributions of P-wave travel time residuals for two earthquakes: a) Svalbard, Norway, and b) SE Afghanistan. The residuals at each station is indicated by a circle. The side of the circle is related to the absolute value of the residual according to the legend. Positive (slow) residuals are shown in red, and negative (fast) residuals in blue. Arrows indicate the approximate incoming direction of the wavefront to the center of the network.

Figure 3. Map of crustal thickness used to compute crustal corrections. Contour lines are drawn every 2 km.

Figure 4. Comparison of results of the tomographic inversion with and without crustal corrections for two shallow layers of the model. Results without crustal corrections are shown in the left panels, and with crustal corrections in the right: a) layer of the model between 75-100 km depth obtained without crustal corrections; b) same as a) but with crustal corrections; c) layer of the model between 125-150 km depth obtained without crustal corrections; d) same as c) but with crustal corrections.

Figure 5. Results of a checkerboard reconstruction test to estimate the resolving power of the arrival time dataset used. The synthetic model consists of two checkerboard patterns located between 100-150 km and 375-425 km. Each checkerboard is made of anomalies with sizes of 1° × 1° and alternating positive and negative velocity anomalies of 2% with

respect to the average P-wave velocity for each layer. a) Reconstructed model for the layer 125-150 km depth. b) Reconstructed model for the layer 400-425 km depth.

Figure 6. Horizontal slices of the P-wave velocity model for different depths. The location of Neogene volcanic rocks is indicated by diamonds. Thin lines indicate the limits of the structural provinces shown in Figure 1. The location of the vertical profiles shown in Figure 7 is indicated as thick lines in b). a) Horizontal slice of the model from 75-100 km. Green circles indicate epicenters of earthquakes from the IGN catalog that occur inside this layer; b) horizontal slice for 125-150 km; c) horizontal slice for 225-250 km; d) horizontal slice for 325-350 km; e) horizontal slice for 475-500 km; f) horizontal slice for 625-650 km. CC: Campo de Calatrava volcanics, Cf: Cofrentes, CG: Cabo de Gata volcanics, Col: Columbretes Islands, GGO: Guelliz, Gourougou and Oujda volcanics, MA: Middle Atlas, IM: Iberian Massif, and MM: Moroccan Meseta.

Figure 7. a) W-E cross section of the model from the Gulf of Cadiz to the Alboran Sea across the Strait of Gibraltar. b) S-N cross section of the model along the -4°W meridian. The location of the profiles is shown in Figure 6b. Green circles are projected hypocenters of earthquakes in the IGN catalog that are closer than 100 km to the profiles.

Figure 8. Geometry of the high velocity anomaly beneath the Alboran region. Lines labeled from 100 to 400 indicate the location of the top of the anomaly/slab for that depth in km (picked as the eastern contour of the +1% velocity anomaly at each depth). The blue area corresponds to the +1% contour of the high velocity anomaly at 450 km depth. The two arrows indicate the propagation path of the proposed northern and southern slab tears. The gray area indicates the region where earthquakes with slab-tear mechanisms occur (according to Ruiz-Constán et al., 2011). Red circles indicate the epicenters of intermediate-depth earthquakes (h > 70 km) in the IGN catalog from 2000-present.

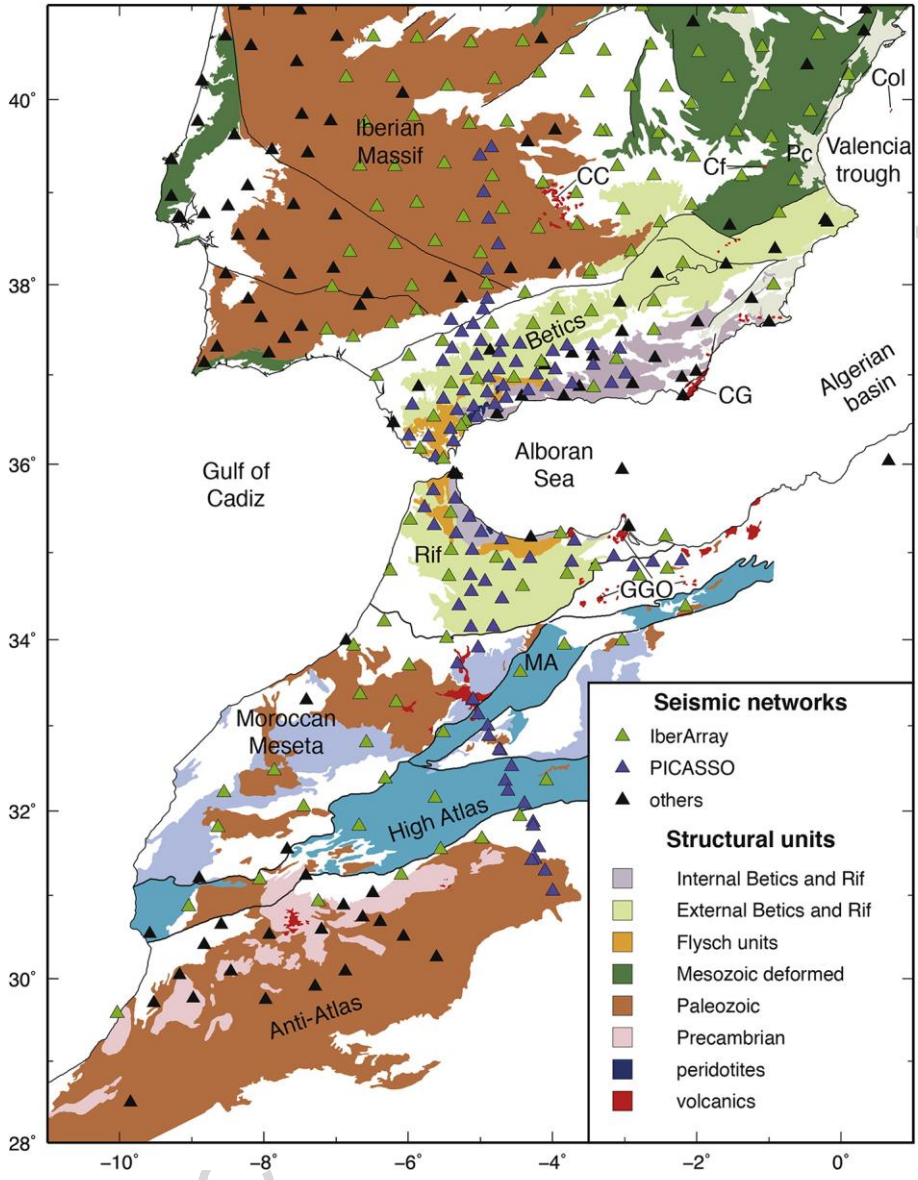
Iberian Massif
CC
Cf
Pc
Col
Valencia trough
Betics
CG
Algerian basin
Alboran Sea
Gulf of Cadiz
Rif
GGO
MA
Moroccan Meseta
High Atlas
Anti-Atlas
40°
38°
36°
34°
32°
30°
28°
−10°
−8°
−6°
−4°
−2°
0°
Seismic networks
IberArray
PICASSO
others
Structural units
Internal Betics and Rif
External Betics and Rif
Flysch units
Mesozoic deformed
Paleozoic
Precambrian
peridotites
volcanics

Figure 1

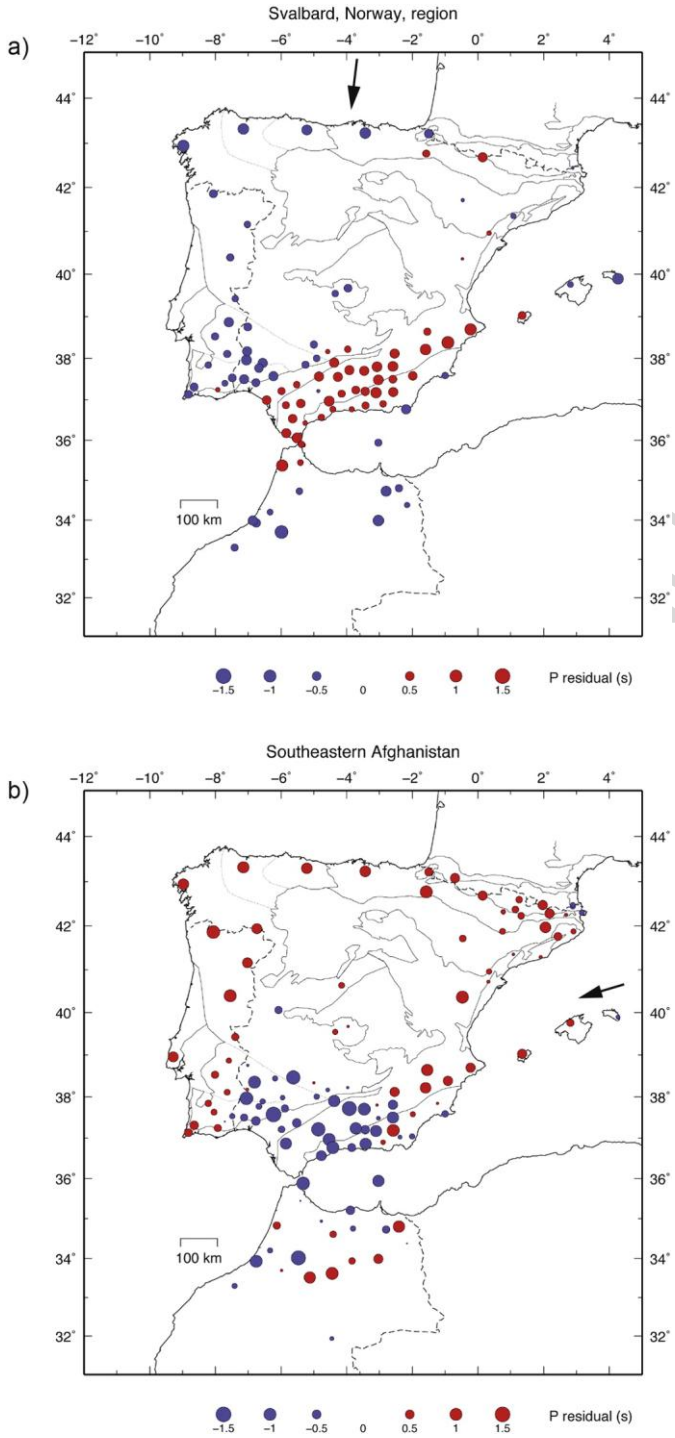

Figure 2

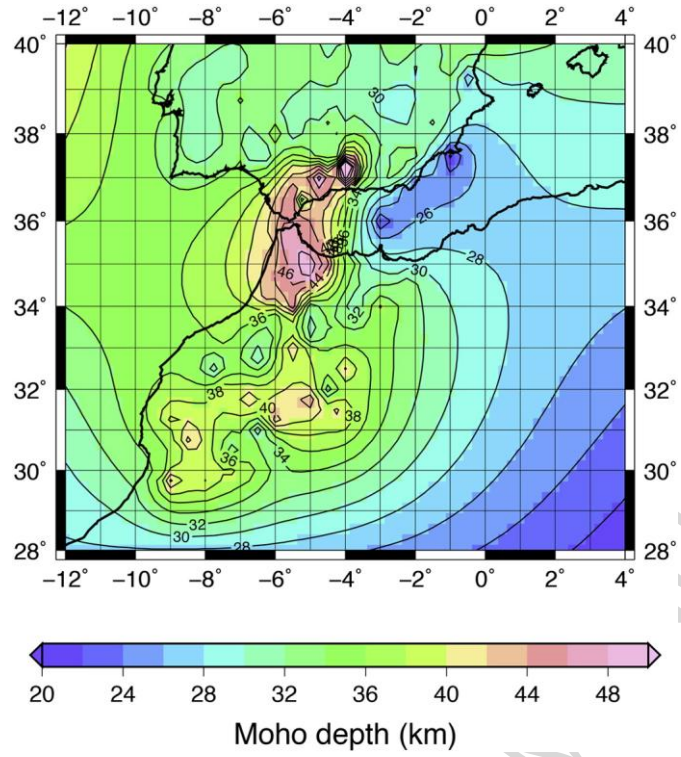

Figure 3

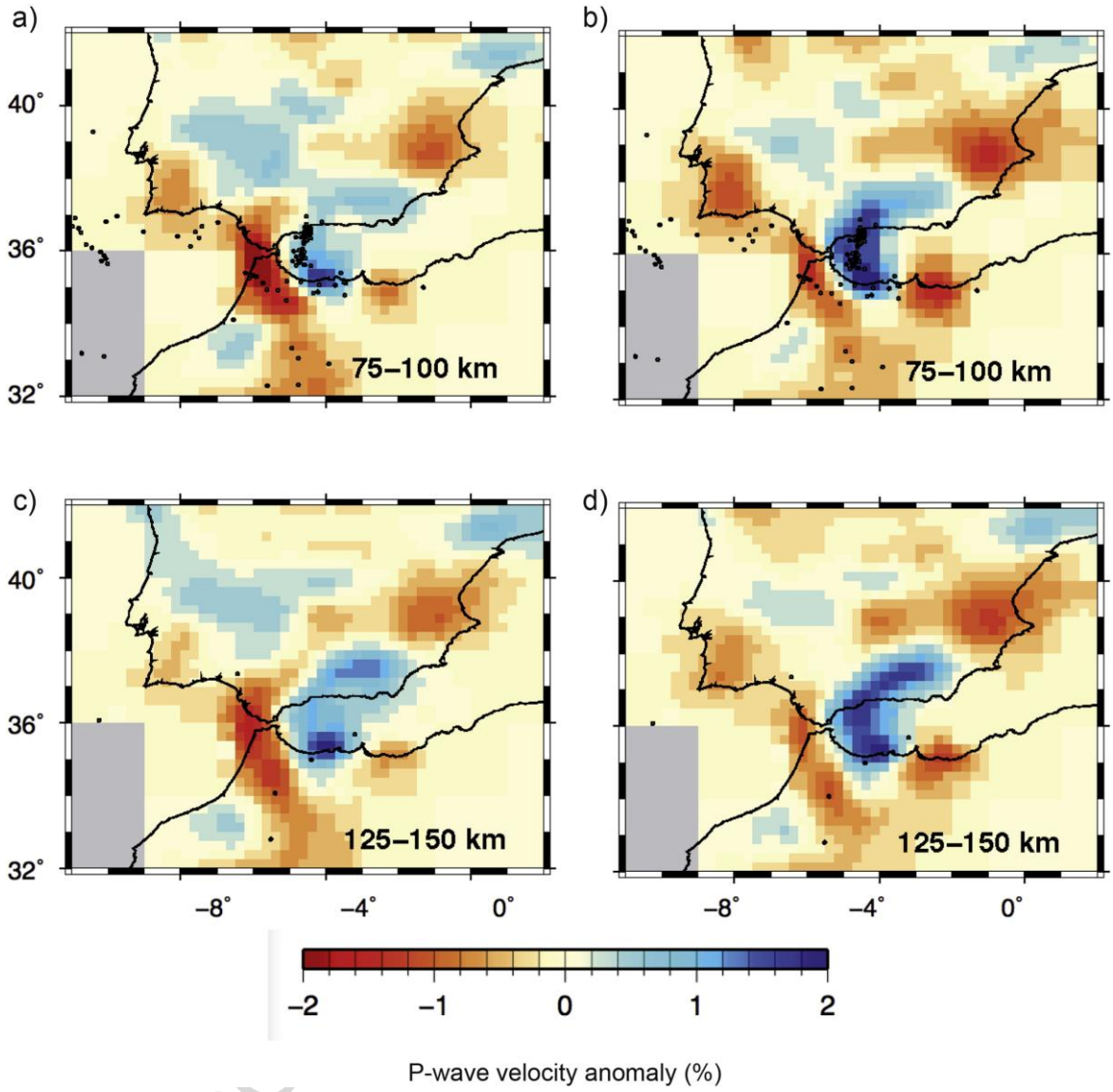

Figure 4

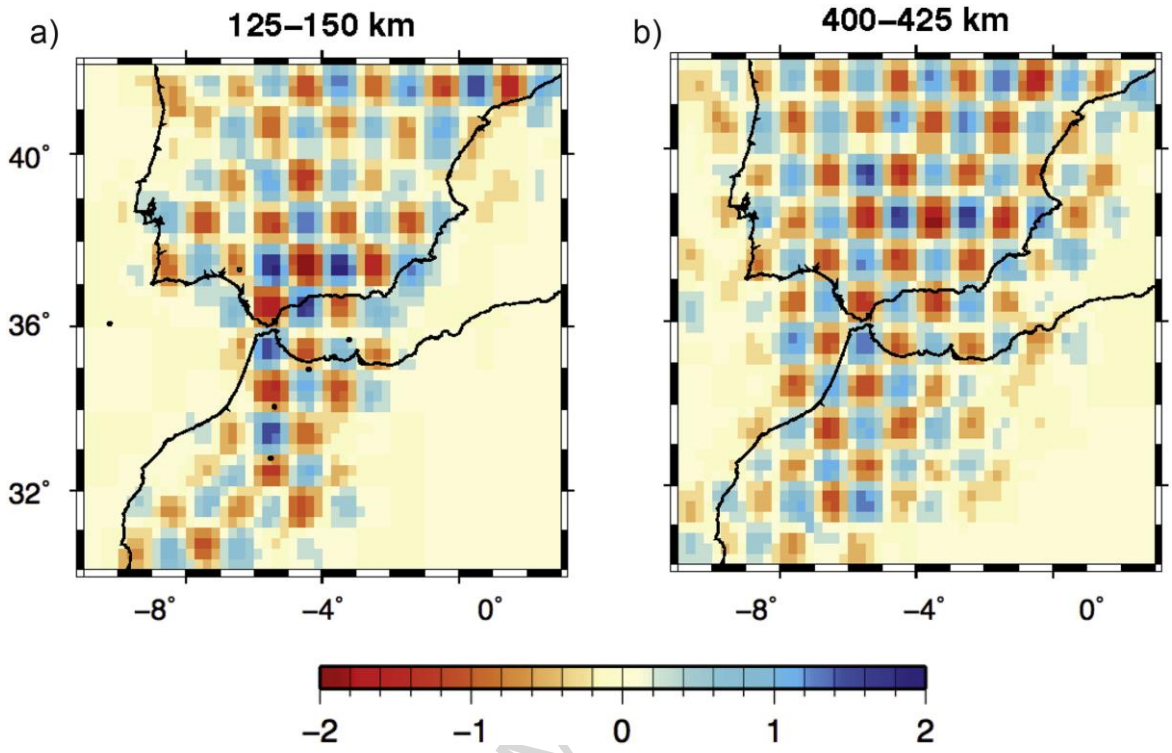

Figure 5

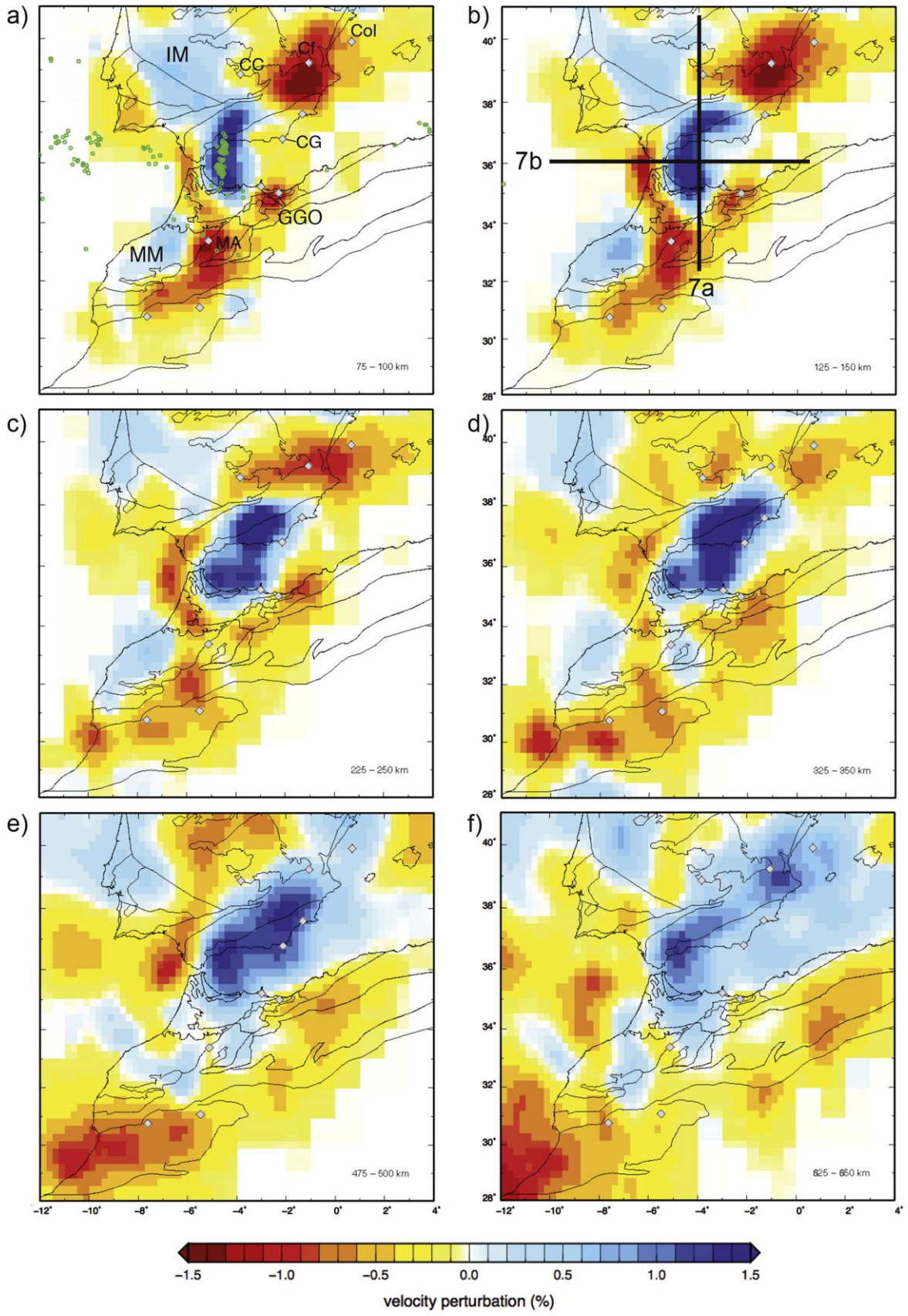
a)
b)
c)
d)
e)
f)
IM
CC
Cf
Col
CG
GGO
MA
MM
7b
7a
75 – 100 km
125 – 150 km
225 – 250 km
325 – 350 km
475 – 500 km
625 – 650 km
−1.5
−1.0
−0.5
0.0
0.5
1.0
1.5
velocity perturbation (%)

Figure 6

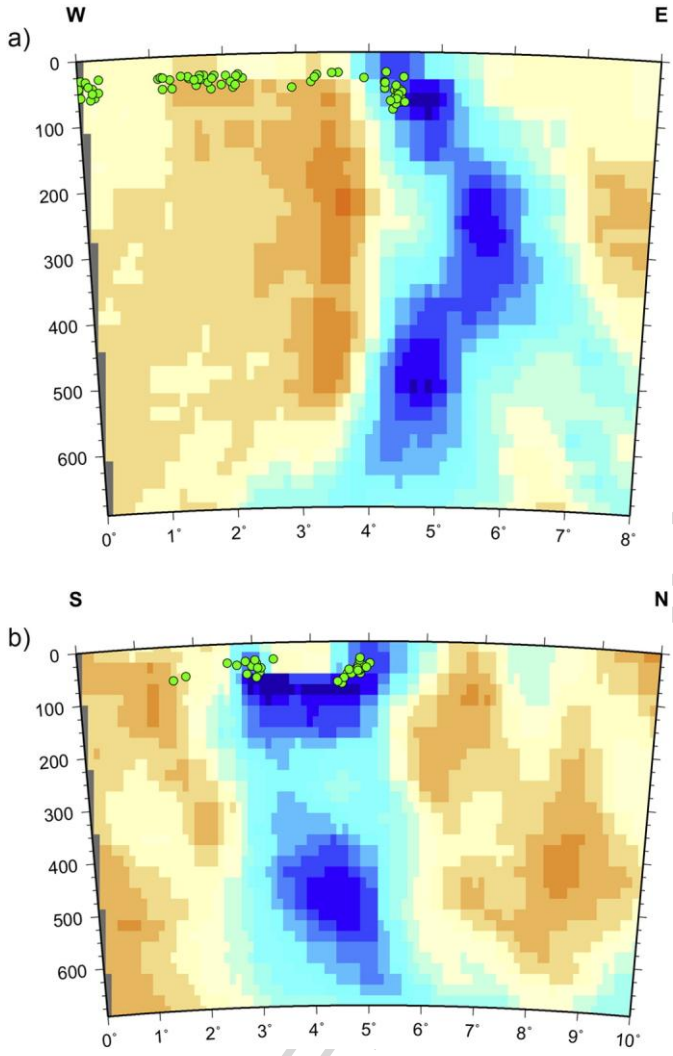

Figure 7

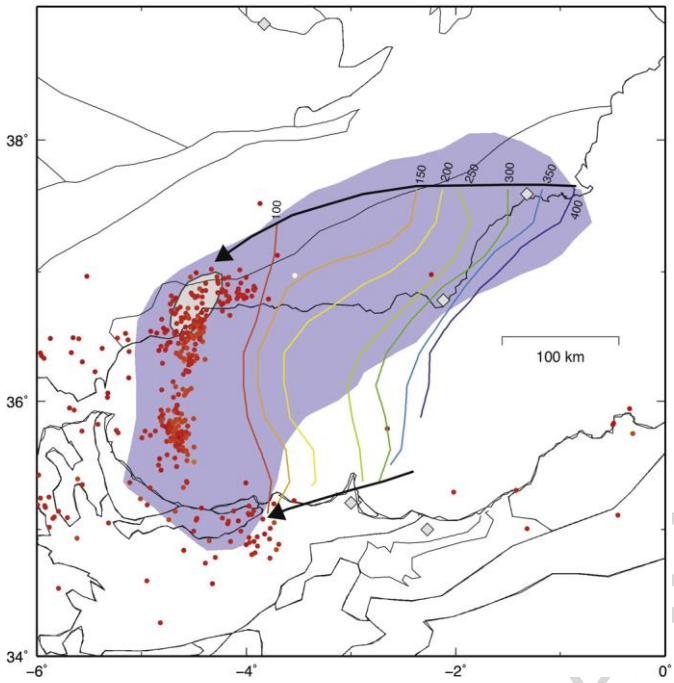

Figure 8

Highlights

New P wave model of Iberia-Africa collision zone

Crustal corrections needed for accurate imaging of the mantle

Seismic structure suggests at least two episodes of subduction